Observations of a structure-forming instability in a dc-glow-discharge dusty plasma

J. R. Heinrich, S.-H. Kim, and R. L. Merlino
Department of Physics and Astronomy, University of Iowa, Iowa City, Iowa, 52242, USA
(Received 31 March 2010; revised manuscript received 13 May 2011; published 5 August 2011)

By adjusting the anode current and axial magnetic strength of a dc-glow-discharge dusty plasma, we have found plasma and dust conditions conducive to dusty plasma structurization, similar to the one discussed theoretically by Morfill and Tsytovich [Plasma Phys. Rep. **26**, 682 (2000)]. The structurization instability leads to the formation of a pattern where the dust suspension transforms into alternating stationary regions of high and low dust densities. We have measured the dependence of the wavelength of the nonpropagating dust density structures on neutral pressure and plasma density and discussed the results in terms of the dispersion relation obtained by D'Angelo [Phys. Plasmas **5**, 3155 (1998)] for an ionization and ion-drag instability. The observations are also considered in light of a recent theoretical prediction by Khrapak *et al.* [Phys. Rev. Lett. **102**, 245004 (2009)] that under certain conditions the effects of the polarization force on dust particles can cause dust acoustic waves to stop propagating, resulting in the formation of aperiodic, stationary dust density structures.

DOI: 10.1103/PhysRevE.84.026403 PACS number(s): 52.27.Lw, 89.75.Kd

I. INTRODUCTION

Dusty (complex) plasmas are plasmas composed of charged dust particles, ions, electrons, and neutral gas atoms. Dusty plasmas exhibit unique behavior such as the formation of voids, i.e., dust-free regions with sharp boundaries [1–4]. Due to the flux of electrons and ions on the surface of dust particles, laboratory dusty plasmas are open systems that require a constant source of ionization to replenish ions and electrons lost to dust particles [5]. Also, the charge on the dust is not fixed but depends on the local plasma properties. These characteristics lead dusty plasmas to be inherently nonequilibrium and nonlinear systems. It is well known that such systems can exhibit self-organization [6–9] and pattern formation [10]. Other structures due to gravitational, polarization, and magnetic forces have also been predicted or observed [11–13]. Structure formation due to dust self-organization is an important process in interstellar dust molecular clouds, protostars, planet formation [11], planetary rings [14], and cometary tails. Other processes, such as nonlinear dust acoustic waves or dust acoustic shocks, can also play a role in triggering particle agglomeration, with important consequences for dust coagulation in astrophysics [15,16].

In plasma physics, spatiotemporal pattern formation has been observed in gas discharges, such as those used for lighting sources or gas lasers [17,18], and in dielectric barrier discharges [19]. D'Angelo predicted spatiotemporal structure formation in dusty plasmas when ionization and ion-drag effects on dust acoustic waves were taken into account [20]. Further analysis of structurization due to ionization and ion-drag effects in dusty plasmas was preformed by Morfill and Tsytovich [9,21]. The mechanism described by D'Angelo [20] and by Morfill and Tsytovich [9,21] can be briefly summarized as follows: If a fluctuation decreases the dust density in a region of a homogeneous dusty plasma, there will be a lower electron absorption in that region, and in turn, a higher electron density. The higher electron density leads to a higher ionization rate, further increasing the plasma density. This results in an enhancement of the outward ion-drag force on the dust, further reducing the dust density in that region. Perhaps the most pronounced observation of this instability is the solitary void formation found in rf discharge dusty plasmas [2]. However, the ionization instability can also lead to the formation of multiple structures in which regions of high dust density are separated by dust voids.

While the ionization instability relies on the ion-drag force to form dust density structures, Khrapak *et al.* [22] showed recently that the effect of the polarization force on dust particles can lead to a decrease in the dust acoustic wave phase velocity and, under certain conditions, the dust acoustic waves cease propagating, resulting in the formation of aperiodic stationary dust density structures.

In this report we present observations of dust structuring in a dusty plasma produced in a dc-glow-discharge plasma. Section II describes the experimental setup and methods, followed by the presentation of the observations in Sec. III. A discussion of the observations in comparison to theoretical predictions is given in Sec. IV. A final summary and conclusions are given in Sec. V.

II. EXPERIMENTAL SETUP AND METHODS

The experiment was conducted using a dc-discharge device, detailed in Fig. 1. Under an argon gas pressure of ∼150 mTorr (20 Pa), a ∼275-V positive bias was applied to a 3.2-cm-diameter electrode disk located on the axis of a horizontal grounded vacuum vessel 90 cm in length by 60 cm in diameter. The discharge current was 16−28 mA. An axial magnetic field of ∼3 mT was applied, which transforms the anode glow discharge (fire-rod [23]) to a cylindrical region protruding several cm from the anode.

Dust particles are introduced into the anode glow plasma from an electrically floating tray located approximately 4 cm below the anode. When the discharge is initially formed, dust particles are lifted off of the tray and become trapped within the plasma. The process of dust incorporation and trapping in the discharge occurs over a time scale of several minutes after which a well-confined dust suspension is formed and the dust tray can be removed. The processes involved in the dust confinement in an anodic plasma have been discussed by Trottenberg *et al.* [24]. The dust particles are confined by a combination of electric forces due to the self-consistently

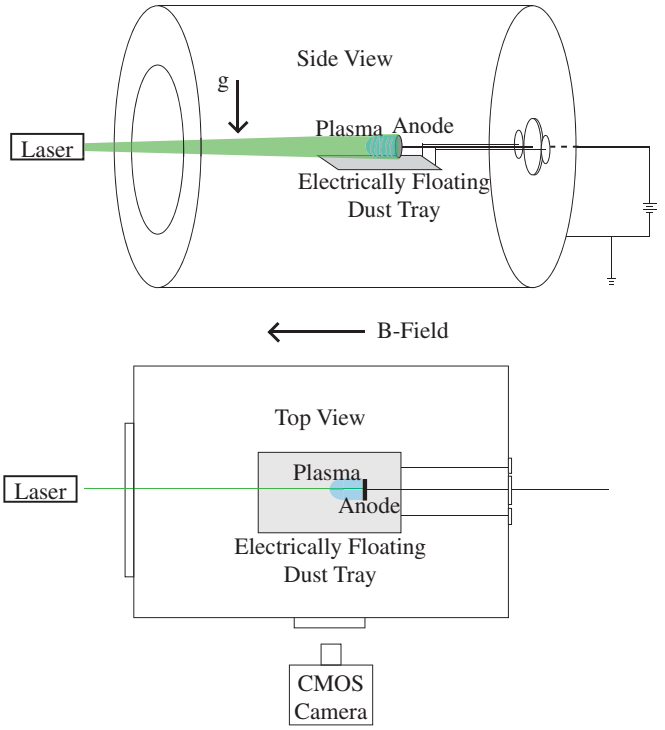

FIG. 1. (Color online) Experimental apparatus. Outline of vacuum chamber and components.

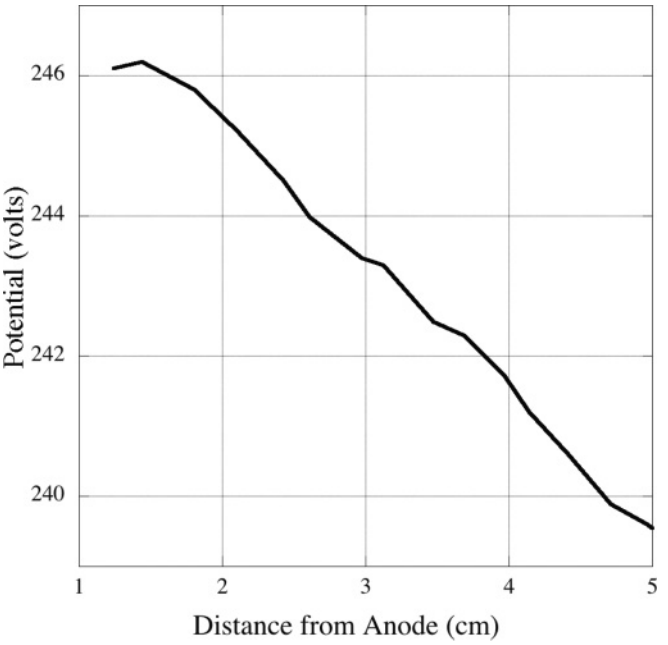

FIG. 2. Axial floating potential measured with an emissive probe in the absence of dust.

formed potential structure of the anode and ion-drag forces. The effects we report here were observed using various dusts and sizes; however, the measurements which will be reported were performed using either spherical iron particles with a narrow size distribution of $1-4\,\mu$m in diameter, or hollow glass microspheres with a broad size distribution extending up to about 30 μm. When non-monodisperse dust particles are used, the distribution of dust sizes that are actually trapped in the suspension may be much narrower than the distribution in the dust reservoir [25]. The dust particles acquire a negative charge due to the preferential collection of the more mobile electrons. For a particular dust radius in microns (a_μ), the dust charge number $Z_d = Q_d/e$ can be estimated using orbital motion limited (OML) theory [25] approximately as $Z_d \approx 4000a_\mu$, for electrons and ion (argon) temperatures of 2.5 and 0.03 eV, respectively.

The plasma potential distribution along the axis from the anode (in the absence of dust) was measured with a floating emissive probe and is shown in Fig. 2. There are no indications of striations or localized potential structures in the initial plasma. The potential falls off monotonically from the anode, resulting in an axial electric field $\sim$180 V/m and was measured with an emissive probe in the absence of dust. This electric field produces an ion flow away from the anode.

The electron temperature and plasma density in the absence of dust particles[1] were measured using a double Langmuir probe and were found to be in the range $T_e \approx 2.2-2.8$ eV, and $n_i \approx (2\text{–}4)\times 10^{14}$ m^{-3} for discharge currents from 15 to 30 mA. By measuring the plasma density through a range of discharge currents with a double probe, the linear dependence of the plasma density on the discharge current was found to be $(1.36 \pm 0.01) \times 10^{16}$ A^{-1} m^{-3}. The double-probe measurements were taken 3 cm from the anode. The ion temperature in these experiments was typically approximately equal to the neutral atom temperature, $T_i \approx T_n \approx 0.03$ eV. Taking $a_\mu = 1\ \mu$m, the Havnes parameter, $Z_d n_d/n_i$, is between 0.1 to 0.2. All the following calculations preserve charge neutrality and use the value of n_i measured in the absence of dust. Although the measurements were taken in the absence of dust, the ion density is not expected to be significantly affected at the observed dust density and the measurements give a very good indication of the ion density in the presence of dust as well as the plasma density dependence on the anode discharge current. The experimental parameters are summarized in Table I.

The dust was observed using a 120-mW, diode pumped solid-state Nd:YAG 532-nm illumination laser expanded into

TABLE I. Experimental parameters.

Parameter	Value	Remarks
n_i	$(2-4) \times 10^{14}$ m^{-3}	Double-probe measurement
n_d	$\sim 1 \times 10^{10}$ m^{-3}	Image analysis
T_i	0.03 eV	Neutral temperature
T_e	2.2–2.8 eV	Measured
E field	$\sim$180 V/m	Emissive probe
B field	3 mT	Measured
Argon pressure	$\sim$150 mTorr	Measured
Z_d (iron)	$\sim$2000–8000e	OML theory
Iron dust diam.	$\sim$1–4 μm	Measured
Hollow glass diam.	$<$30 μm	Measured

[1]Electrical probes usually cannot be inserted into a dusty plasma because of the substantial disturbance they cause to the dust suspension, as documented, for example, in Thompson *et al.* [25]

a vertical sheet and a Photron (FASTCAM 1024 PCI) CMOS camera for capturing 1-megapixel images at frame rates of 60 to 1000 fps. The dust density is proportional to the intensity of the scattered light so that fluctuations in density can be directly determined from fluctuations in image intensity as discussed in [26].

III. OBSERVATIONS

The formation of a stationary dust density structure was observed for discharge currents above 16 mA. For discharge currents <10 mA propagating dust acoustic waves (DAWs) were spontaneously excited due to the relative drift of the ions through the dust. When the discharge current was increased above 16 mA, the topology of the dust cloud was changed, with the cloud splitting into a primary cloud of higher dust density and a secondary cloud of lower dust density farther from the anode. The dust in the lower density cloud spontaneously self-organized into a stationary pattern of alternating regions of high and low dust density. The high density regions were much broader than the low density regions. The stationary structures had a wavelength ~5 mm, with typically three to four regions of enhanced dust density. Figure 3(a) shows a single frame video image taken with the cloud illuminated by a thin vertical sheet of 532-nm laser light. From video images of the structure obtained at several vertical laser sheet slices, we observed that the structures were not planar, but were arranged as nested conical structures. Figure 3(b) shows spatial profiles of the scattered laser light intensity (proportional to the dust density) corresponding to a 2-mm window through the center of the structure. Several profiles, taken over an image sequence of 33 s at 3.3-s intervals, are shown. The relatively small differences between profiles indicate the robustness of the stationary structures. The structures remained relatively unchanged for the entire length of time that the device was on. Multiple images of the structured dust cloud were obtained by positioning the laser sheet through a series of cross-sectional slices. These images were used to produce a tomographic reconstruction of the three-dimensional cloud as shown in Fig. 4. While the geometry of the structured cloud showed variation with radial position (which can be explained by the conical shape of the dust cloud), the wavelength of the structure was relatively independent of the radial position, best seen by examining the bright middle striation marked in Fig. 4. The data shown in Figs. 3 and 4 were taken using spherical iron particles, but very similar results were obtained using hollow glass microspheres, kaolin powder, and spherical copper particles, showing that the self-organized structurization does not depend critically on the type of dust material, which determines the mass, etc. Similar observations were also obtained in helium plasmas, although at higher neutral pressures.

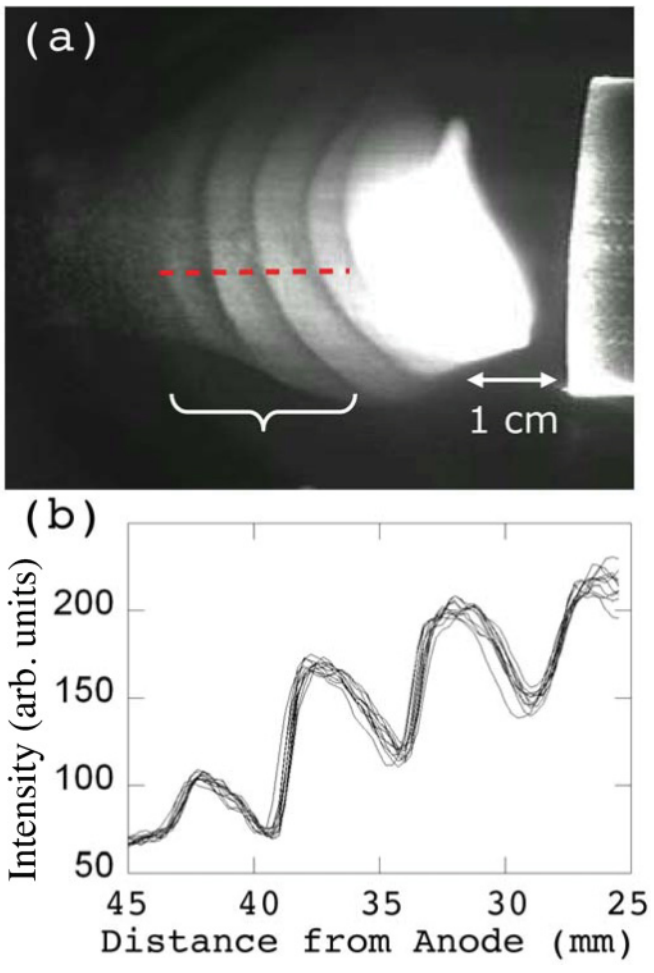

FIG. 3. (Color online) Zero-frequency mode. (a) Single frame image of the stationary dust structure illuminated by a thin vertical laser sheet. (b) Ten spatial intensity profiles of scatter laser light across dashed line in (a) taken at 3.3-s intervals.

The dependence of the spatial scale (wavelength) of the structures on discharge parameters (discharge current and neutral pressure) was investigated. Figure 5 shows single frame video images and corresponding intensity profiles for structures formed in a dusty plasma using hollow glass microspheres for discharge currents of 19, 22, and 25 mA. There is a systematic decrease in structure wavelength with increasing discharge current. A summary plot of wavelength vs discharge current is shown in Fig. 6. The origin of the dashed line (theory) will be discussed later. Figure 7 shows the dependence of the structure wavelength on neutral argon pressure. The wavelength decreases with increasing pressure. The data of Fig. 6 may also be seen as a decrease in wavelength with increasing plasma density, since the plasma density increases as the discharge current is increased. The data of Fig. 7 may be seen as a decrease in wavelength with an increase in ionization rate as the ionization rate increases with neutral pressure.

IV. DISCUSSION

In summary, we have presented observations of spontaneous self-organized structurization in a dc-glow-discharge dusty plasma. This structurization is characterized by the formation of stationary alternating regions of high dust density and low dust density (partial voids). There are no electric potential structures (e.g., striations) in the plasma prior to the trapping of the dust suspension that might account for the dust structures. Once formed, these structures remain stationary and stable. If these stable dust structures are

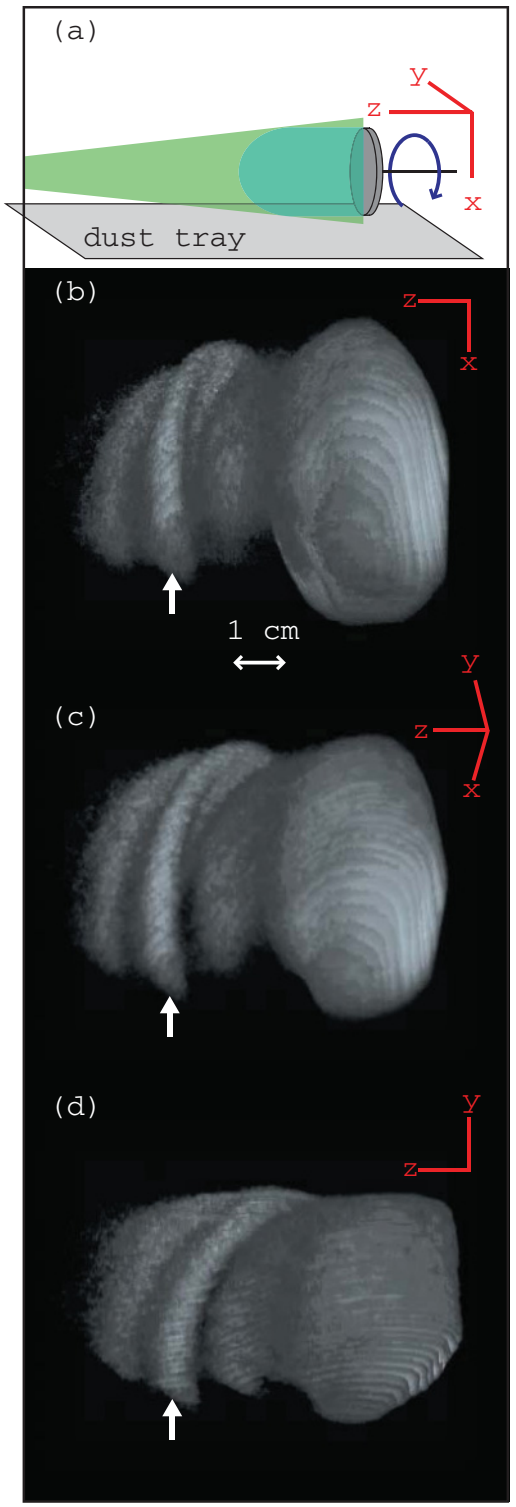

FIG. 4. (Color online) Tomographic reconstruction of dust cloud with structure formation. The axis orientation is shown in (a). The cloud is illuminated by the laser sheet in the x-z plane. Three-dimensional views can be seen in (b)–(d) as the point of view is rotated [in the direction shown by the blue arrow in (a)]. The tomographic reconstruction shows the nonplanar nested conical shell structure of the zero-frequency dust density striations. A well-formed dust density striation that illustrates the relative independence of the wavelength on radial position is marked in (b)–(d). The anode was removed from the images to improve clarity.

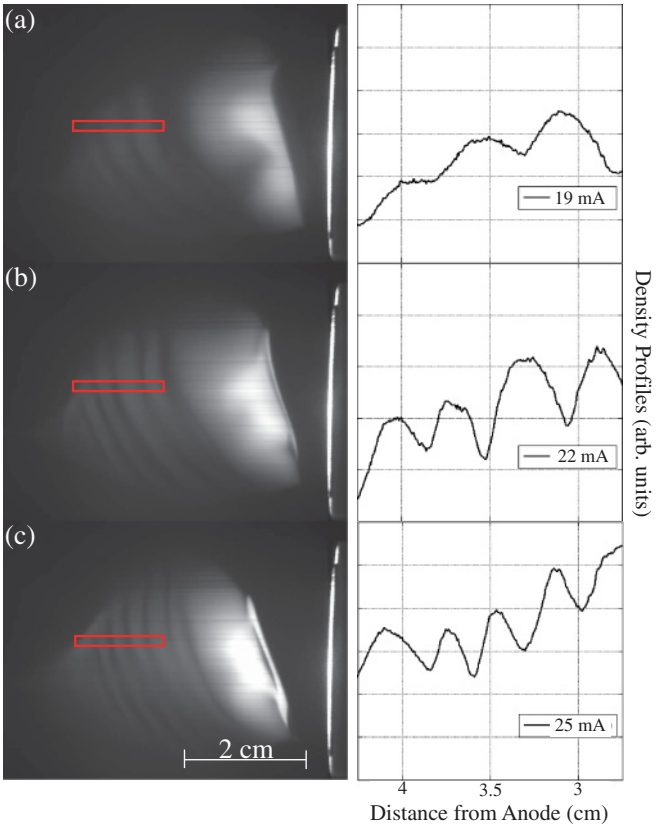

FIG. 5. (Color online) Zero-frequency structure formations at different discharge currents. Images averaged over 200 frames and recorded at 60 fps. The electrode current is set at (a) 19, (b) 22, and (c) 25 mA. Corresponding density profiles are shown to the right over the selected regions. The contrast and brightness of the image have been adjusted to improve clarity. Taken with hollow glass particles.

disturbed by, for example, the insertion of a floating object, they spontaneously re-form once the object is removed. The dust structures were formed in argon and helium discharges, and using various types of dust materials: spherical iron and copper particles, glass microspheres, and irregularly shaped particles of aluminum silicate (kaolin). The formation process thus appears to be rather robust with respect to plasma and dust conditions, with the exception that the structurization was observed when the discharges were operated at discharge currents greater than about 15 mA, and the structures became more pronounced as the discharge current was increased. There are two mechanisms which have been discussed theoretically which may give rise to stationary dust density structures in dusty plasmas. These are (A) the ionization instability with ion-drag [9,20] and (B) the polarization force [22].

A. Ionization and ion-drag instability

Morfill and Tsytovich [9] argue that a unique feature of dusty plasmas is that the dust charge is not fixed but depends on the local plasma conditions, and, since the dust particles absorb electrons and ions in the plasma, an ionization source is required to sustain the plasma. This "openness" property of dusty plasmas supports self-organization and structurization. As discussed in the Introduction, the presence of ionization and

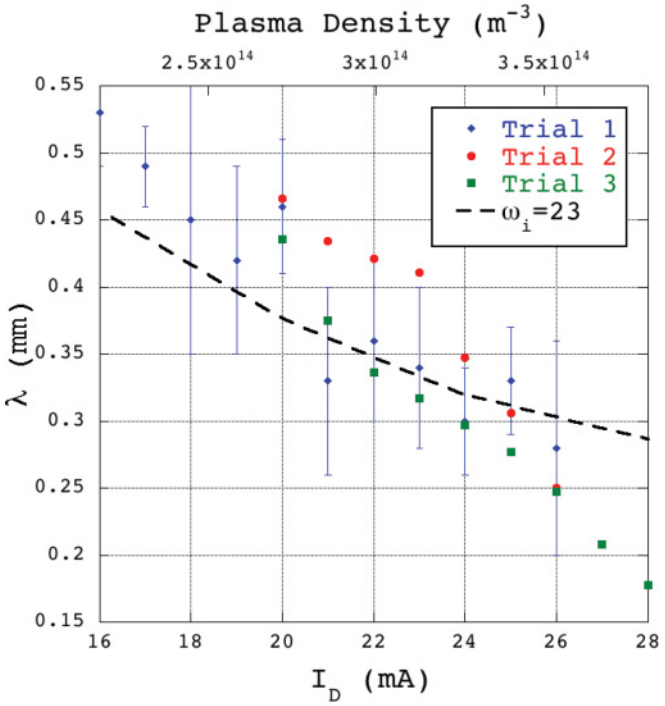

FIG. 6. (Color online) Wavelength vs discharge current and plasma density. Separate experimental runs are denoted by their trial number. Wavelengths were obtained by averaging over the density peaks. The dashed line is taken from D'Angelo's model as described in Sec. IV A for a growth rate of $\omega_i = 23$ (rad s^{-1}). Taken with hollow glass particles.

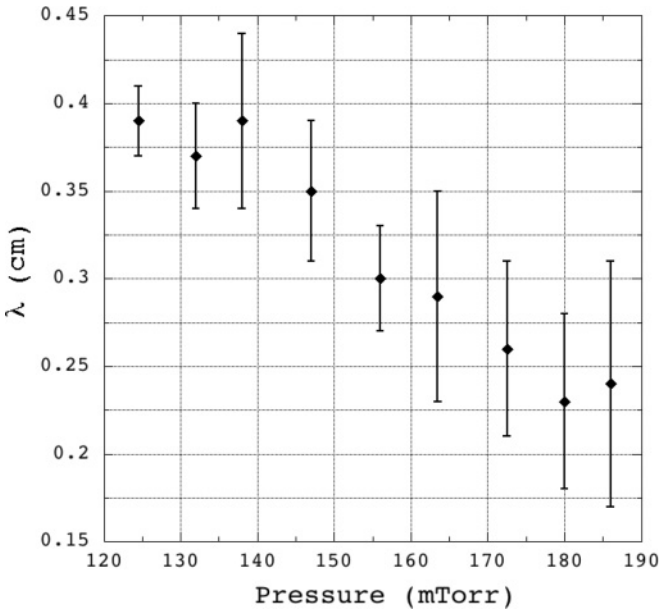

FIG. 7. Observed wavelength dependence of zero-frequency dust density structures on neutral gas pressure. Taken at a discharge current of 22 mA with glass microspheres. Additional boundary effects and the finite cloud size may contribute to nonmonotonic features in the wavelength vs neutral gas density trend. Error bars indicate the range of wavelengths observed in the dust cloud at a given pressure.

the ion-drag force on dust particles leads to instability, which in the nonlinear stage produces dust clumps separated by dust voids. Morfill and Tsytovich [9] show that the characteristic size of the structures which are formed (the wavelength corresponding to maximum growth) are $\lambda_{\rm MT}$: λ_{Di}^2/a, where $\lambda_{Di} = (\varepsilon_o k_B T_i/e^2 n_i)^{(1/2)}$ is the ion Debye length, and a is the dust size. For an ion temperature and density of $k_B T_i \approx 0.03$ eV and $n_i \approx 3 \times 10^{14}$ m^{-3} and a in the range of 1–4 μm, $\lambda_{\rm MT} \sim$ 1–5 mm, which corresponds roughly to the sizes of the structures which we have observed. The inverse scaling of $\lambda_{\rm MT}$ with ion density is also in qualitative agreement with the observations presented in Fig. 6.

A quantitative comparison of the observations with predictions of the ionization and ion-drag instability model was made by solving the dispersion relation derived by D'Angelo [20], using parameters appropriate for our experimental conditions. D'Angelo's dispersion relation was obtained using the continuity and momentum equations for the ions and dust particles, the Boltzmann relation for the electrons, and the charge neutrality condition. The ion continuity equation included a source term for the creation of ions through ionization of neutral atoms by a small (compared to the thermal electrons) component of fast electrons, and a loss term due to absorption of ions on the dust and to the walls of the plasma container. The ionization source term contained an electron energy dependent ionization cross section. The ionization instability occurs since for acoustic-like perturbations, regions of elevated electron density also correspond to regions of elevated plasma potential. Since the ionization cross section is a rapidly increasing function of electron energy just above the ionization potential, electrons in the wave crests will be more energetic than those in the wave troughs and thus ionization proceeds more rapidly in the wave crests. The dust momentum equation included momentum loss due to dust-neutral collisions and a term due to the drag of the ions on the dust particles.[2] The perturbed electric field in the wave crests causes the ions to move outward from the crests, dragging the dust particles with them, thus forming regions of depressed dust density (voids). D'Angelo showed (see Fig. 5 of Ref. [20]) that if the ion-drag force exceeds a critical value, there is a transition from damped and propagating dust acoustic waves to a growing, nonpropagating dust density perturbation (a zero-frequency instability). It should be noted that in D'Angelo's model, the dust is taken to be cold with a constant charge eZ_d, and ion-neutral collisions and ion viscosity are ignored.

The dispersion relation was solved for dust of radius $a = 1$ μm, a dust-neutral collision frequency of 10 s^{-1}, and for an ion-dust collision frequency in the range of 0.09–0.15 s^{-1} depending on the ion density, which is controlled experimentally by the discharge current. The ion-dust collision frequency

[2]D'Angelo uses the 1992 model of Barnes *et al.* [28], for the ion-drag force. The Barnes *et al.* model uses as a cutoff of the collection impact parameter the Debye length. The range of the interaction has been shown to extend well beyond this limit and considerable work has been done recently in an attempt to provide a more accurate expression for the orbit force [27,29]. The calculation of the ion-drag force requires as input the ion-drift speed. This was obtained using the expression from Robertson and Sternovsky [30]. For the parameters in our experiment we found $v_{id}/v_{Ti} = 0.6$.

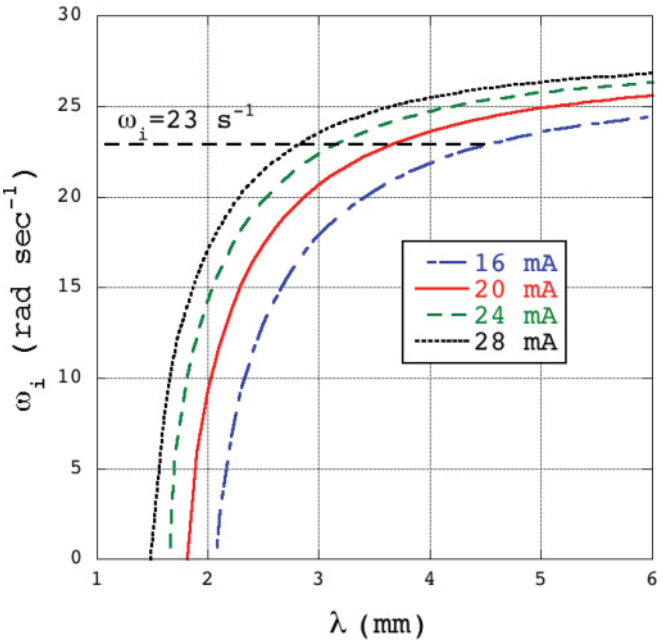

FIG. 8. (Color online) Growth rate vs wavelength predicted by the D'Angelo model for the ionization and ion-drag instability. Growth rates correspond to a zero-frequency mode with discharge currents of 16–28 mA, corresponding to plasma densities of (2.2–3.8)$\times 10^{14}$ m^{-3}. Calculated for dust grains with radii $a_\mu = 1$ μm at 150 mTorr and an electric field of 180 V/m. Dashed line indicates the growth rate taken for the dashed line in Fig. 6.

was calculated using the theory of Khrapak *et al.* [27]. For these parameters and with wavelengths greater than 1.5 mm, growing zero-frequency modes were found, as shown in Fig. 8 by plots of the growth rate ω_i vs the mode wavelength λ for various values of the discharge current. Thus for typical values of the parameters in our experiments, the model predicts growing nonpropagating modes; and furthermore, the results of Fig. 6 indicate that growth shifts to shorter wavelengths as the discharge current (plasma density) is increased, as shown by the dashed line, which is in reasonable agreement with the measured wavelengths. The time scales for the appearance of the dust structures is also in line with the calculated growth rates.

Both the Morfill and Tsytovich [9] and D'Angelo models for the ionization and ion-drag instability predict the presence of sharp boundaries between the dust clouds separated by dust voids. In the experiments, however, we did not observe the formation of dust voids but rather regions of dust compressions separated by regions of dust rarefactions. There are effects not included in the theories, however, that may lead to a smoothing of the boundaries; these effects include finite dust temperatures and non-monodisperse dust.

B. Nonpropagating, growing dust acoustic perturbations due to the effect of the polarization force

Khrapak *et al.* [22] have shown that if the effect of the polarization force acting on dust grains is taken into account in the linear stability analysis of dust acoustic waves, under certain conditions, discussed below, the dust acoustic waves cannot propagate, but rather nonpropagating dust density perturbations are found. The polarization force on dust grains occurs for grains in a nonuniform plasma, and is due to the deformation of the Debye shielding cloud surrounding the dust grains, which gives rise to an additional local electric field and force on the grain in the direction of decreasing Debye length. When this force is included in the fluid analysis, the usual dispersion relation for DA waves is altered by the presence of a new term $(1 - \Re)$, so the phase speed for dust acoustic modes is given by

$$w/k = \sqrt{1 - \Re}\, C_{\mathrm{DA}} \tag{1}$$

where $C_{\mathrm{DA}} = \omega_{pd}\lambda_{Di} = \sqrt{Z_d^2 n_d k_B T_i / m_d n_d}$ is the dust acoustic speed, and $\Re = \Re(\beta_T)$, where $\beta_T = \rho_o/\lambda_{Di}$ where $\rho_o = e^2 Z_d/4\pi\varepsilon_o k_B T_i$ is the Coulomb radius of interaction between thermal ions and the grain. For $\Re < 1$, the phase speed is simply decreased. However, for $\Re > 1$, the dispersion relation predicts a transition to a growing but nonpropagating perturbation. Due to the effect of nonlinear screening around the dust grain, the value of β_T must be found numerically, and Khrapak *et al.* [22] found that the onset of the unstable nonpropagating mode occurs at $\beta_T \approx 6.4$. This allows us to consider if, under the conditions of our experiments, growing nonpropagating modes might be expected to occur. The parameter β_T scales as $\beta_T \propto Z_d\sqrt{n_i}/(k_B T_i)^{3/2}$ and since the grain charge number $Z_d \propto a k_B T_e$, we have that $\beta_T \propto a k_B T_e n_i^{1/2}/(k_B T_i)^{3/2}$. Since $k_B T_e$ and $k_B T_i$ remain relatively constant as the plasma density changes; and since the plasma density is proportional to the discharge current I_D, we have finally that $\beta_T = B a I_D^{1/2}$, where B is a constant. Using $\beta_T = 6.4$, a stability plot in the (a, I_D) plane, is shown in Fig. 9, in which the shaded region indicates the parameter region where the unstable growing perturbations

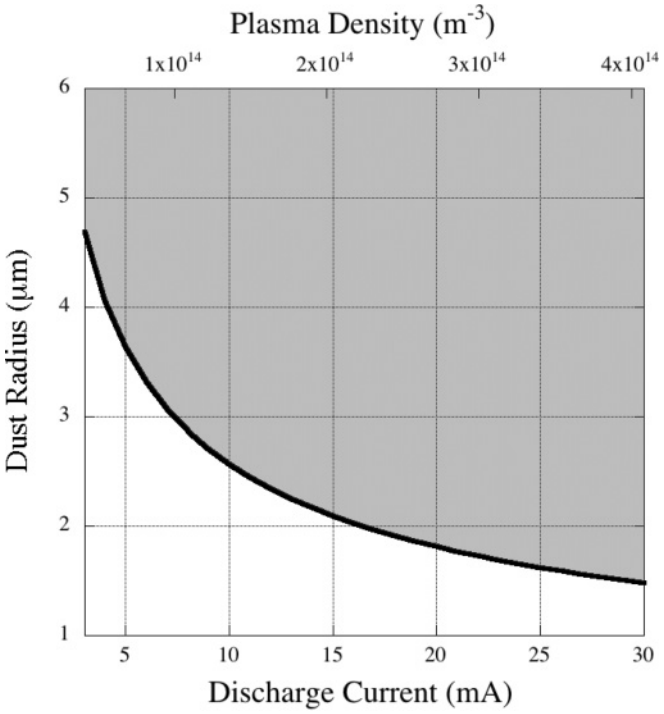

FIG. 9. Onset of polarization instability. The shaded portion is the parameter region where $\beta_t > 6.4$ and stationary dust acoustic waves are predicted to exist [22].

are predicted to occur. Stationary dust structures were observed for $I_D > 16$ mA, with grains in the size range (radius) of ~ 2.2 μm, which falls in the region where the zero-frequency, growing modes are predicted to occur.

Although, this comparison indicates that the effects of the polarization force on the dust grains could possibly explain the observations, the theory neglects a number of important other effects that will need to be considered in a more detailed comparison. For example, dust-neutral collisions, ion-neutral collisions, and ion-dust collisions (ion-drag force) have not been included at this point.

V. CONCLUSION

We have presented experimental observations made in a dc-glow-discharge dusty plasma of the formation of stationary dust density structures. The ordered structures are stable and have many of the features of the *structurization instability* discussed by Morfill and Tsytovich [9]. A detailed description of the observed structure was made as well as a discussion of and comparison to two theoretical mechanisms that predict the formation of nonpropagating dust density perturbations—one based on the ionization and ion-drag instability [20] and the other based on the effect of the polarization force on dust grains [22]. While the theoretical calculations are based on linear theory so that they do not indicate what the nonlinear state of the structures might be, both models are able to account for features of the observed structures.

ACKNOWLEDGMENTS

We thank V. N. Tsytovich as well as S. A. Khrapak for helpful communications. This work was supported by DOE Grant No. DE-FG01-04ER54795.

[1] G. Praburam and J. Goree, Phys. Plasmas **3**, 1212 (1996).
[2] D. Samsonov and J. Goree, Phys. Rev. E **59**, 1047 (1999).
[3] J. Goree, G. E. Morfill, V. N. Tsytovich, and S. E. Vladimirov, Phys. Rev. E **59**, 7055 (1999).
[4] H. Feng, Y. Mao-Fu, and W. Long, Chin. Phys. Lett. **21**, 121 (2004).
[5] V. Tsytovich, G. Morfill, S. Vladimirov, and H. Thomas, *Elementary Physics of Complex Plasmas* (Springer, Berlin, 2008), p. 144.
[6] D. Winske, IEEE Trans. Plasma Sci. **29**, 191 (2001).
[7] V. E. Fortov, A. P Nefedov, O. F. Petrov, A. A. Samarian, and A. V. Chernyschev, Phys. Rev. E **54**, R2236 (1996).
[8] W. Masood, A. Mirza, and S. Nargis, Phys. Plasmas **15**, 103703 (2008).
[9] G. Morfill and V. Tsytovich, Plasma Phys. Rep. **26**, 682 (2000).
[10] J. Gollub and L. Langer, Rev. Mod. Phys. **71**, S396 (1999).
[11] B. P. Pandey, K. Avinash, and C. B. Dwivedi, Phys. Rev. E **49**, 5599 (1994).
[12] A. V. Ivlev, G. E. Morfill, H. M. Thomas, C. Räth, G. Joyce, P. Huber, R. Kompaneets, V. E. Fortov, A. M. Lipaev, V. I. Molotkov, T. Reiter, M. Turin, and P. Vinogradov, Phys. Rev. Lett. **100**, 095003 (2008).
[13] J. Zamanian, G. Brodin, and M. Marklund, New J. Phys. **11**, 073017 (2009).
[14] O. Havnes, T. Aslaken, F. Melandso, and T. Nitter, Phys. Scr. **45**, 491 (1992).
[15] J. Heinrich, S.-H. Kim, and R. L. Merlino, Phys. Rev. Lett. **103**, 115002 (2009).
[16] C.-R. Du, H. M. Thomas, A. V. Ivlev, U. Konopka, and G. E. Morfill, Phys. Plasmas **17**, 113710 (2010).
[17] Y. P. Raizer, *Gas Discharge Physics* (Springer, Berlin, 1991).
[18] E. Lozneanu, V. Popescu, S. Popescu, and M. Sanduloviciu, IEEE Trans. Plasma Sci. **30**, 30 (2002).
[19] E. Ammelt, D. Schweng, and H.-G. Purins, Phys. Rev. Lett. A **179**, 348 (1993); W. Breazeal, K. M. Flynn, and E. G. Gwinn, Phys. Rev. E **52**, 1503 (1995); U. Kogelschatz, IEEE Trans. Plasma Sci. **30**, 1400 (2002); E. L. Gurevich, A. L. Zanin, A. S. Moskalenko, and H.-G. Purwins, Phys. Rev. Lett. **91**, 154501 (2003).
[20] N. D'Angelo, Phys. Plasmas **5**, 3155 (1998).
[21] V. Tsytovich, Aust. J. Phys. **51**, 763 (1998).
[22] S. A. Khrapak, A. V. Ivlev, V. V. Yaroshenko, and G. E. Morfill, Phys. Rev. Lett. **102**, 245004 (2009).
[23] T. An, R. L. Merlino, and N. D'Angelo, J. Phys. D **27**, 1906 (1994).
[24] T. Trottenberg, D. Block, and A. Piel, Phys. Plasmas **13**, 042105 (2006).
[25] C. O. Thompson, N. D'Angelo, and R. L. Merlino, Phys. Plasmas **6**, 1421 (1999).
[26] A. I. S. Annibaldi, U. Konopka, S. Ratynskaia, H. Thomas, G. Morfill, A. Lipaev, O. P. V. Molotkov, and V. Fortov, New J. Phys. **9**, 327 (2007).
[27] S. A. Khrapak, V. Nosenko, G. E. Morfill, and R. Merlino, Phys. Plasmas **16**, 044507 (2009).
[28] M. S. Barnes, J. H. Keller, J. C. Forster, J. A. O'Neill, and D. K. Coultas, Phys. Rev. Lett. **68**, 313 (1992).
[29] S. A. Khrapak, A. V. Ivlev, G. E. Morfill, and H. M. Thomas, Phys. Rev. E **66**, 046414 (2002).
[30] S. Robertson and Z. Sternovsky, Phys. Rev. E **67**, 046405 (2003).